

**Local symmetry breaking in paramagnetic insulating (Al,V)<sub>2</sub>O<sub>3</sub>**

P. Pfalzer, J. Will, A. Nateprov, Jr., M. Klemm, V. Eyert, and S. Horn  
*Institut für Physik, Universität Augsburg, Universitätsstraße 1, 86159 Augsburg, Germany*

A. I. Frenkel  
*Physics Department, Yeshiva University, 245 Lexington Avenue, New York, New York 10016*

S. Calvin  
*Naval Research Lab, Code 6340, Washington, DC 20375*

M. L. denBoer  
*Department of Physics, Hunter College, City University of New York, 695 Park Avenue, New York, New York 10021*  
 (Received 2 December 2001; published 30 August 2002)

The local structure of (Al<sub>0.06</sub>V<sub>0.94</sub>)<sub>2</sub>O<sub>3</sub> in the paramagnetic insulating (PI) and antiferromagnetically ordered insulating (AFI) phase has been investigated using hard and soft x-ray absorption techniques. It is shown that (1) on a local scale, the symmetry of the vanadium sites in both the PI and AFI phases is the same and (2) the vanadium-3*d*-oxygen-2*p* hybridization, as gauged by the oxygen 1*s* absorption edge, is the same for both phases, but distinctly different from the paramagnetic metallic phase of pure V<sub>2</sub>O<sub>3</sub>. These findings can be understood in the context of a recently proposed model which relates the long-range monoclinic distortion of the antiferromagnetically ordered state to orbital ordering, if orbital short-range order in the PI phase is assumed. The measured anisotropy of the x-ray absorption spectra is discussed in relation to spin-polarized density functional calculations.

DOI: 10.1103/PhysRevB.66.085119

PACS number(s): 71.30.+h, 61.10.Ht, 71.27.+a, 78.70.Dm

**INTRODUCTION**

The metal-insulator transition (MIT) in V<sub>2</sub>O<sub>3</sub> has been intensively investigated and discussed for many years as an example of a classical Mott transition. However, such a picture is blurred by the complexity of the V<sub>2</sub>O<sub>3</sub> phase diagram<sup>1</sup> which involves magnetic and structural transitions coinciding with the MIT, as a function of temperature, doping (Cr, Al, Ti), pressure, and oxygen stoichiometry. At room temperature pure V<sub>2</sub>O<sub>3</sub> is in a paramagnetic metallic (PM) phase which x-ray diffraction (XRD) shows to be trigonal. At about 180 K there occurs a transition to an antiferromagnetically insulating (AFI) monoclinic phase. Doping with Cr or Al results in the formation of a paramagnetic insulating (PI) phase. The lattice parameters change but long-range trigonal symmetry is preserved, as indicated by XRD.<sup>2,3</sup> The role of electronic correlations in the interplay between changes in the physical structure, the magnetic properties, and the electronic structure at the various transitions needs further investigation. It is still not certain whether the electronic transition is driven by structural changes or vice versa. Although recent calculations combining the local density approximation with local density approximation with dynamical mean-field theory (LDA + DMFT)<sup>4</sup> show the importance of electronic correlations in a description of the electronic structure, a description of the MIT in V<sub>2</sub>O<sub>3</sub> must take into account the relationship between physical structure and the electronic and magnetic properties of the system.

The Mott-Hubbard picture of V<sub>2</sub>O<sub>3</sub>, in particular a description in terms of a one-band Hubbard model,<sup>5</sup> is based on a level scheme of Castellani *et al.* for the electronic structure of V<sub>2</sub>O<sub>3</sub>.<sup>6</sup> The crystal field generated by the O octahedron

splits the V 3*d* states into upper *e<sub>g</sub>* and lower *t<sub>2g</sub>* states, and the latter are further split into *a<sub>1g</sub>* and *e<sub>g</sub><sup>π</sup>* states due to the trigonal symmetry of the lattice. Interactions between nearest vanadium neighbors along the *c* direction (vertical pairs) split the *a<sub>1g</sub>* states into bonding and antibonding molecular orbitals. According to Castellani *et al.* the bonding *a<sub>1g</sub>* orbital is fully occupied while the antibonding *a<sub>1g</sub>* orbital shifts energetically above the *e<sub>g</sub><sup>π</sup>* states. This leaves only one electron per vanadium atom to occupy the *e<sub>g</sub><sup>π</sup>* states, leading to orbital degeneracy, which is susceptible to a degeneracy-lifting process such as the Jahn-Teller effect or orbital ordering. Indeed, Bao *et al.*<sup>7,8</sup> suggested that such orbital ordering occurs in V<sub>2</sub>O<sub>3</sub>. This conclusion was based on neutron scattering experiments which show disagreement between the propagation vector characterizing the AFI phase and the propagation vector expected from magnetic short-range order in the PM and PI phases of pure V<sub>2</sub>O<sub>3</sub> and its alloys. The latter propagation vector is identical to that of a spin density wave in vanadium-deficient V<sub>2</sub>O<sub>3</sub>. The suggested orbital ordering would distinguish the AFI phase of V<sub>2</sub>O<sub>3</sub> from all the other phases and prevent a unified description of the MIT in this compound. The validity of Castellani's model has been called into question by soft x-ray absorption<sup>9,10</sup> and band structure calculations.<sup>11</sup> Near-edge x-ray-absorption fine-structure (NEXAFS) measurements of the V 2*p* and O 1*s* edges provide information on the unoccupied states near the Fermi level. Müller *et al.* concluded from such a NEXAFS study of the different phases of V<sub>2</sub>O<sub>3</sub> and (V,Cr)<sub>2</sub>O<sub>3</sub> that all the insulating phases have, within experimental error, identical local electronic structures.<sup>9</sup> In addition, angular-resolved NEXAFS measurements in the metallic and insulating phases of V<sub>2</sub>O<sub>3</sub> are inconsistent with the assumption that the

first excited states are purely  $e_g^\pi$ . Rather, the isotropy of the absorption spectra observed in the metallic phase suggests the first excited states are a mixture of  $e_g^\pi$  and  $a_{1g}$ , while the anisotropy observed in the insulating phases suggests these states have increased  $a_{1g}$  character. These conclusions were confirmed by LDA+ $U$  band-structure calculations by Ezhov *et al.*<sup>11</sup> and NEXAFS studies by Park *et al.*<sup>10</sup> Using a model fit to the V  $2p$ , Ezhov *et al.* showed that orbital occupancy of the  $e_g^\pi$  states is larger than 1 and changes at both MIT's. This renders the one-band Hubbard model<sup>5</sup> often applied to the MIT in  $V_2O_3$  inadequate.

Important for a unified view of the MIT in  $V_2O_3$  is the understanding of the relationship between electronic, magnetic, and structural changes at the MIT. Recently, a model was proposed<sup>12,13</sup> that takes into account degrees of freedom of molecular orbitals formed by vertical V-V pairs and their interaction within the  $ab$  plane, offering a consistent picture of the magnetic and structural properties of the AFI phase.

In this paper we show using EXAFS and NEXAFS techniques that, on a local scale, the structural and electronic properties of the AFI and PI phases are the same. This fact is attributed to short-range orbital order in the PI phase, consistent with recent model calculations<sup>12,13</sup> and the characteristics of magnetic short-range order observed by neutron scattering.<sup>7</sup> Spin-polarized density functional theory calculations presented here reflect the anisotropy of the O  $2p$  density of states observed in the insulating phases of the  $V_2O_3$  phase diagram.

## EXPERIMENTAL AND THEORETICAL METHODOLOGY

Measurements were performed on an Al-doped  $V_2O_3$  single crystal about 2.5 mm by 1.5 mm by 1 mm grown by chemical transport using  $TeCl_4$  as transport agent and a mixture of  $V_2O_3$  and  $Al_2O_3$  powder corresponding to a nominal concentration  $x=0.1$  in  $(V_{1-x}Al_x)_2O_3$ . Energy-dispersive x-ray scattering showed that the actual Al concentration in the single crystal was 6 at.%, presumably due to a lower transport rate of Al compared to vanadium during crystal growth. XRD showed the expected trigonal structure with lattice parameters  $c_{hex}=13.81(1)$  Å and  $a_{hex}=4.985(5)$  Å, both smaller than those found by Joshi *et al.* ( $c_{hex}\approx 13.89$  Å and  $a_{hex}\approx 5.00$  Å at 6.2 at.%).<sup>14</sup> The resulting  $c/a$  ratio of 2.7703 is much smaller than in the metallic phase (2.828). Resistivity measurements, the small value of the  $c/a$  ratio, and the Al concentration show the sample was in the PI phase at room temperature. The transition from PI to AFI occurred at 165 K as determined by magnetic susceptibility measurements using a Quantum Devices superconducting quantum interference device (SQUID) magnetometer. Laue diffraction measurements were performed on the single crystal at room-temperature and at 77 K. The room temperature trigonal symmetry was, as expected, broken at low temperature.

A pure, slightly vanadium-deficient  $V_2O_3$  single crystal was measured as a reference. Laue diffraction and magnetic susceptibility measurements showed that the single crystal was of high quality with a sharp MIT at 100 K. The resistiv-

ity of this crystal was monitored during the EXAFS experiment.

The EXAFS measurements were performed at beamline X23B at the National Synchrotron Light Source at Brookhaven National Laboratory. Spectra at different temperature points above and below the transition temperatures of the pure and doped samples were taken using a closed-cycle helium cryostat. The EXAFS spectra taken above the transition were measured before and after the crystals passed through the transition. No differences were observed, ruling out the influence of cracks on the measurements. For the pure compound this was also verified by only small changes in the geometry factor in the *in situ* resistance measurement. Cracks in the doped sample are less likely since the AFI-PI transition is characterized by a much smaller unit-cell volume change than the AFI-PM transition. The sample was held under vacuum to reduce thermal leakage and air absorption and prevent water condensation. The x-ray absorption spectra were measured in fluorescence yield mode using a Lytle detector;<sup>15</sup> background radiation was filtered by a Ti foil. In fluorescence mode self-absorption effects may strongly damp the EXAFS amplitude even at normal incidence. As the primary effect of self-absorption is to reduce the EXAFS amplitude,<sup>16,17</sup> but leave the phase unchanged, the distances of neighboring atoms obtained by EXAFS, which are determined largely by the phase, are unaffected. We corrected for self-absorption using a generalization of the method of Tröger *et al.*<sup>16,18</sup> to large detector surfaces, as described elsewhere.<sup>17</sup> This correction is quite reliable, as was shown in Ref. 17 by demonstrating that for Al-doped  $V_2O_3$  the absorption was isotropic in the  $ab$  plane after the correction, as expected for trigonal symmetry.

For the EXAFS measurements the sample was oriented so that the  $(11\bar{2}0)$  plane (in hexagonal notation) was the surface perpendicular to the incident beam. In this geometry the orientation of the polarization vector  $\vec{E}$  of the incoming x rays with respect to the hexagonal  $c$  axis can be changed by rotating the sample around the surface normal. Measurements were made with  $\vec{E}$  parallel and perpendicular to  $\vec{c}_{hex}$ . As described by Frenkel *et al.*,<sup>19</sup> this facilitates measuring the two different components of the anisotropic absorption coefficient:

$$\mu = \mu_{\perp} \sin^2 \theta + \mu_{\parallel} \cos^2 \theta,$$

where  $\mu_{\perp}$  ( $\mu_{\parallel}$ ) is the absorption coefficient for  $\vec{E}$  perpendicular (parallel) to  $\vec{c}_{hex}$  and  $\theta$  is the angle between  $\vec{E}$  and  $\vec{c}_{hex}$ . Since different scattering paths contribute to  $\mu_{\perp}$  and  $\mu_{\parallel}$ , measurement of these two independent quantities achieves better separation of paths. After correcting for self-absorption as described above, standard EXAFS analysis was performed. For the Fourier transform a window in  $k$  space from  $3 \text{ \AA}^{-1}$  to  $12 \text{ \AA}^{-1}$  was used ( $k$  being the wave vector of the photoelectron).

Measured spectra were compared to model spectra calculated with FEFF8.<sup>20</sup> The calculation requires estimated atomic positions, provided by models of the structure. To construct these structural models we used the lattice parameters provided by our XRD measurements. Then, for the trigonal

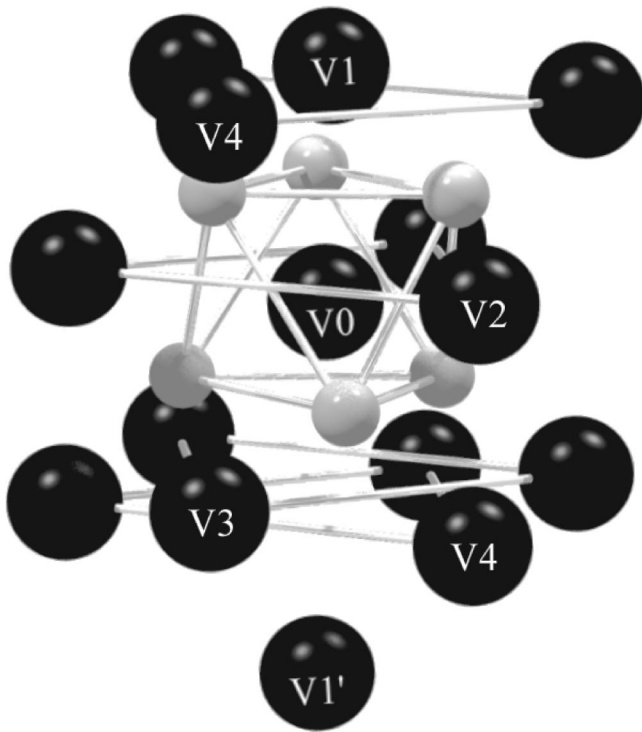


FIG. 1. Local structure of  $V_2O_3$ . Black (gray) spheres represent vanadium (oxygen) ions. Only those oxygen ions which form an octahedron around the central vanadium atom  $V_0$  are shown. The hexagonal  $c$  axis is along the line  $V_1'-V_0-V_1$ .

model, we used the atomic positions tabulated by Wyckoff<sup>21</sup> for the pure compound. For the monoclinic model, we started with the measured hexagonal lattice parameters and tilted the  $c_{hex}$  axis by  $1.995^\circ$ , the same amount as in the AFI phase of undoped  $V_2O_3$ ,<sup>22</sup> to reproduce the monoclinic distortion. The resulting pseudohexagonal lattice vectors were converted to monoclinic ones using the conversion matrix of Ref. 23. Relative atomic positions for the monoclinic phase were also taken from Ref. 23. The structure refinement was performed by varying the interatomic distances to all vanadium atoms up to the fourth nearest neighbor, as shown in Fig. 1, as well as to the nearest two shells of oxygen atoms. A few double-scattering paths with high scattering amplitudes were included in the fits. The nearest oxygen shell forms a (distorted) octahedron around the absorbing vanadium atom  $V_0$  and is responsible for the well-separated peak of the Fourier transformed spectra between 1 and 2 Å. Fitting was carried out in  $r$  space using  $k^3$  weighting.

NEXAFS measurements on the O  $1s$  edge were performed under ultrahigh vacuum at the U41-1/PGM beamline at the BESSY 2 storage ring using the same crystal in the same geometry as for the EXAFS measurements. The signal was monitored by measuring the total electron yield; this is somewhat surface sensitive, so care was taken to prepare and maintain clean surfaces characteristic of the bulk.

The experiments were complemented by electronic structure calculations based on density functional theory (DFT) in the LDA. The calculations used the augmented-spherical-wave (ASW) method in its scalar-relativistic implementation,<sup>24,25</sup> which was already applied in Ref. 4.

The present study included the paramagnetic metallic  $V_2O_3$ , paramagnetic insulating  $(V_{0.962}Cr_{0.038})_2O_3$ , and antiferromagnetic insulating  $V_2O_3$  phases using the crystal-structure data of Dernier<sup>26,27</sup> as well as Dernier and Marezio.<sup>23</sup> Note that, since DFT is a ground-state theory, differences between the phases were taken into account only via the different crystal structure. In order to study the effect of spin polarization separately from the monoclinic distortion in the AFI state, a complementary set of calculations with enforced spin degeneracy was performed for this structure.

In order to account for the openness of the crystal structures, empty spheres, i.e., pseudoatoms without a nucleus, were included to model the correct shape of the crystal potential in large voids. Optimal empty-sphere positions and radii of all spheres were automatically determined by the recently developed sphere geometry (SGO) algorithm.<sup>28</sup> As a result, 8 and 16 empty spheres with radii ranging from  $1.78a_B$  to  $2.42a_B$  were included in the trigonal and monoclinic cells, respectively, keeping the linear overlap of vanadium and oxygen spheres below 16.5%. The basis set comprised V  $4s$ ,  $4p$ ,  $3d$  and O  $2s$ ,  $2p$  as well as empty-sphere states. Fast self-consistency was achieved by an efficient algorithm for convergence acceleration.<sup>29</sup> Brillouin zone sampling was done using an increasing number of  $\vec{k}$  points ranging from 28 to 2480 and from 108 to 2048 points within the respective irreducible wedges, ensuring convergence of the results with respect to the fineness of the  $k$ -space grid.

## RESULTS

In Fig. 2 we compare the EXAFS (in  $k$  space) of a pure  $V_2O_3$  sample and the Al-doped sample above (dashed lines) and below (solid lines) their respective transition temperatures. For the Al-doped sample EXAFS spectra were measured with the polarization vector  $\vec{E}$  oriented along and perpendicular to the hexagonal  $c$  axis. The EXAFS is very similar for both orientations for both the PI and AFI phases of this sample [see Figs. 2(a) and 2(b)], indicating that this transition, involving a long-range monoclinic distortion and magnetic order, is accompanied by only minor changes in local structure. In contrast, for pure  $V_2O_3$ , the large differences in the EXAFS oscillations apparent in Fig. 2(c) show that the local environment of the absorbing atoms is very different above and below the MIT. For the PI and AFI phases of the Al-doped sample, small differences are apparent at high  $k$ ; these presumably are due to the distinctly different Debye-Waller factors at the measuring temperatures of 30 K and 180 K, respectively.

Fitting procedures, further discussed below, provide local interatomic distances which confirm that the local structure is virtually the same in the PI and AFI phases of the Al-doped sample, but also in the AFI phase of pure  $V_2O_3$ . The fit also shows that both the PI and AFI phases of the Al-doped  $V_2O_3$  have a local symmetry which corresponds to a monoclinic lattice. Figure 3 compares the measured EXAFS (in  $r$  space, where  $r$  is the interatomic distance) for both orientations of  $\vec{E}$  to  $\vec{c}_{hex}$  to spectra derived from model calculations for monoclinic and trigonal structures. It is evident

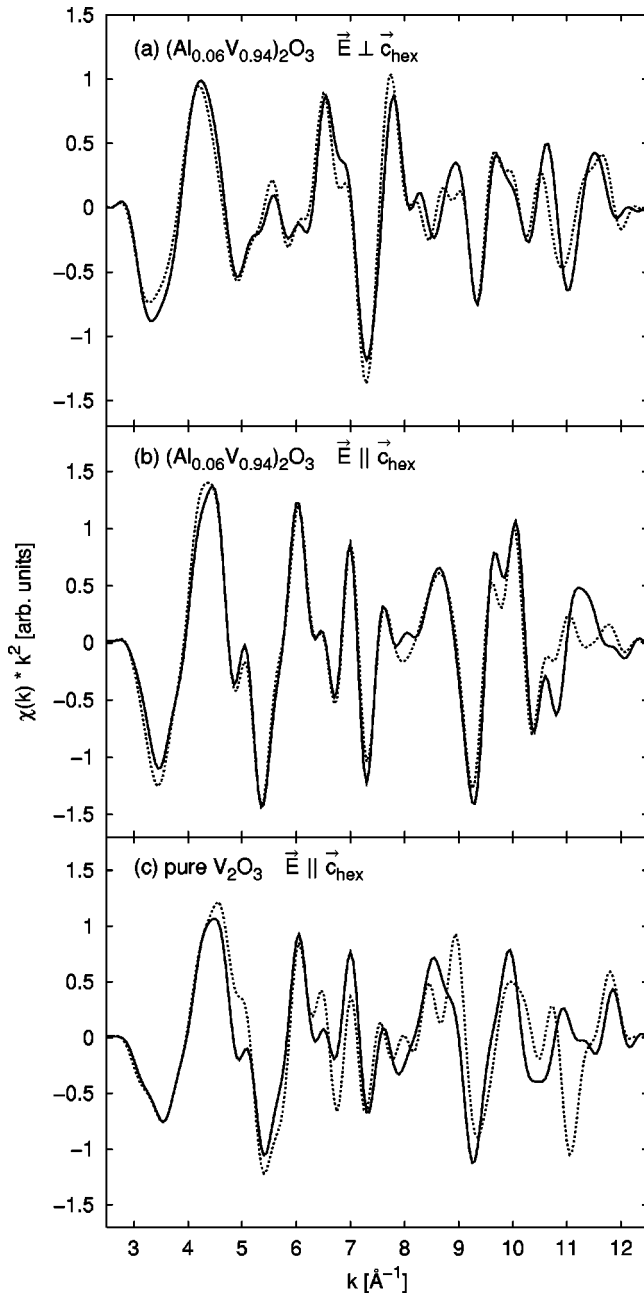


FIG. 2. EXAFS spectra of  $(\text{Al}_{0.06}\text{V}_{0.94})_2\text{O}_3$  in  $k$  space. The spectra above (dashed line) and below (solid line) the PI to AFI transition are virtually the same for Al-doped  $\text{V}_2\text{O}_3$  for both  $\vec{E} \perp \vec{c}_{hex}$  and  $\vec{E} \parallel \vec{c}_{hex}$  [(a) and (b)], while pronounced changes are observed in pure  $\text{V}_2\text{O}_3$  which is in the PM state at room temperature (c), showing that the two insulating phases have virtually identical local physical structure which differs from that of the metal.

that the monoclinic model fits the data better. The trigonal model (long-dashed lines) fits the data very poorly in the PI phase at 180 K as well as in the AFI phase at 30 K, while the monoclinic model (dotted lines) fits the data very well in both cases, especially doing a much better job in describing the distorted oxygen octahedron (peak at 1.7 Å) and the next vanadium neighbors ( $V_1$  and  $V_1'$ , contributions are around 2.2 Å and below 4 Å in Fig. 3). This visual observation is

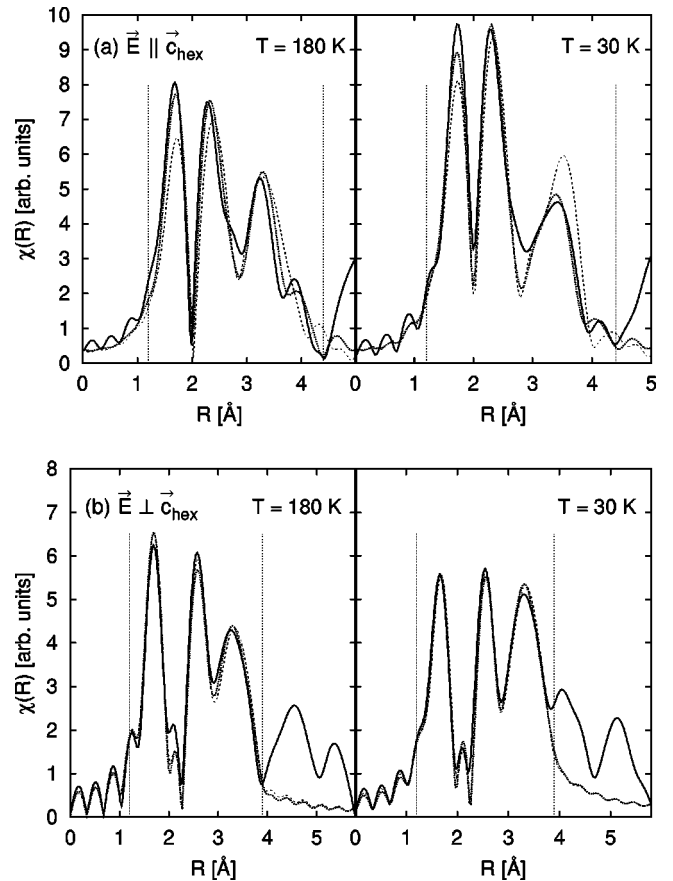


FIG. 3. FT magnitudes of the EXAFS spectra of  $(\text{Al}_{0.06}\text{V}_{0.94})_2\text{O}_3$  (solid line) compared to calculated EXAFS using a monoclinic model (dotted lines) and a trigonal model (long-dashed lines), for two geometries: (a)  $\vec{E} \parallel \vec{c}_{hex}$ , in which significant differences between the models are expected. The monoclinic model fits the data much better than the trigonal one in both the PI ( $T=180$  K) and AFI ( $T=30$  K) phases. (b)  $\vec{E} \perp \vec{c}_{hex}$ . In this geometry many paths contribute and little difference is expected between the models, as observed. Dotted vertical lines indicate the  $R$  range used in the fit. The positions of the peaks are not corrected by the scattering phase shifts (0.3–0.5 Å).

confirmed by the fact that the reliability factor of the trigonal model is 0.06, while that of the monoclinic model is 0.02. The better fit of the monoclinic model than the trigonal model is particularly apparent in the  $\vec{E} \parallel \vec{c}_{hex}$  orientation. This is expected because the EXAFS measured in this orientation is more sensitive to the structural differences between the phases; the major effect of the reduction in symmetry during the transition from PI or PM to AFI is a tilt of the  $c_{hex}$  axis and a “rotation” of  $\text{V}_0$ - $\text{V}_1$  next-neighbor pairs, all located along this axis. This orientation also achieves good separation of scattering paths, since there is only a single V next-neighbor atom ( $V_1$  in Fig. 1) along the  $c_{hex}$  axis. In fact, the main contribution to the scattered intensity at 2.2 Å in Fig. 3(a) is due to the  $\text{V}_0$ - $\text{V}_1$  single-scattering path. The broad peaks in the spectra taken with the polarization vector  $\vec{E}$  of the x rays perpendicular to the  $c_{hex}$  axis [Fig. 3(b)] contain a large number of paths and therefore fit

TABLE I. Distances  $r$  from the central ion  $V_0$  to nearby V ions (as labeled in Fig. 1) for various V compounds and Debye-Waller factors  $\sigma^2$  for the EXAFS fits presented in Fig. 3. The model for the interatomic distances in  $(Al_{0.06}V_{0.94})_2O_3$  uses hexagonal lattice vectors measured by XRD and relative atomic positions, assuming a trigonal (T) (Ref. 26) or monoclinic (M) (Ref. 23) lattice. (For the monoclinic lattice the distances to the  $V_2$ ,  $V_3$ , and  $V_4$  ions become nondegenerate and hence are identified separately in the table.) Distances for  $V_2O_3+Cr$ , specifically  $(Cr_{0.038}V_{0.962})_2O_3$ , in the PI phase were measured by Dernier (Ref. 26). Values for the AFI phase of pure  $V_2O_3$  are calculated from the monoclinic lattice vectors and atomic positions published by Dernier and Marezio (Ref. 23). See text.

Ion (see Fig. 1)	$(Al_{0.06}V_{0.94})_2O_3$					$V_2O_3+Cr$	$V_2O_3$
	Model		Experiment		AFI $\sigma^2$ [ $\text{\AA}^2$ ]	PI $r$ [ $\text{\AA}$ ]	AFI $r$ [ $\text{\AA}$ ]
	T $r$ [ $\text{\AA}$ ]	M $r$ [ $\text{\AA}$ ]	PI $r$ [ $\text{\AA}$ ]	$\sigma^2$ [ $\text{\AA}^2$ ]			
$V_1$	2.72	2.72	$2.76 \pm 0.03$	$0.001 \pm 0.0006$	$2.79 \pm 0.03$	$0 \pm 0.0006$	2.74
$V_2$	(i)	2.86	$2.96 \pm 0.02$		$2.91 \pm 0.02$		2.86
	(ii)	2.91	$2.97 \pm 0.02$	$0.001 \pm 0.0007$	$2.93 \pm 0.02$	$0.001 \pm 0.0009$	2.88
	(iii)	3.00	$3.10 \pm 0.02$		$3.05 \pm 0.02$		2.99
$V_3$	(i)	3.44	$3.44 \pm 0.03$		$3.42 \pm 0.04$		3.44
	(ii)	3.44	$3.46 \pm 0.03$		$3.44 \pm 0.04$		3.46
$V_4$	(i)	3.62	$3.69 \pm 0.02$	$0.003 \pm 0.0009$	$3.72 \pm 0.02$	$0.006 \pm 0.001$	3.63
	(ii)	3.69	$3.71 \pm 0.02$		$3.81 \pm 0.02$		3.73
	(iii)	3.72	$3.79 \pm 0.02$		$3.82 \pm 0.02$		3.74

equally well to both models with a reliability factor of 0.02.

Table I lists the distances from a central reference ion, labeled  $V_0$  in Fig. 1, to nearby V ions for the various phases of the  $V_2O_3$  compounds. The values measured by EXAFS for the PI and AFI phases are those obtained using the fits shown in Fig. 3. The distances to the  $V_3$  and  $V_4$  nearest neighbors were consistently determined from the fits to the spectra with  $\vec{E}$  parallel  $\vec{c}_{hex}$  and  $\vec{E}$  perpendicular  $\vec{c}_{hex}$ , while the distances to  $V_2$  and  $V_1$  were taken from the  $\vec{E} \perp \vec{c}_{hex}$  and  $\vec{E} \parallel \vec{c}_{hex}$  spectra alone, respectively, since both the  $V_1$  and  $V_2$  neighbors only contribute to one kind of spectrum significantly. The relative atomic positions, which determine the splitting of the distances to  $V_2$ ,  $V_3$ , and  $V_4$  in the monoclinic phase, were taken from Ref. 23 and only the average distances of the shells taken into account in the fit were varied. For comparison, we include interatomic distances calculated for  $(Al_{0.06}, V_{0.94})_2O_3$  obtained using hexagonal lattice vectors measured by XRD and relative atomic positions, assuming a trigonal<sup>26</sup> and monoclinic lattice.<sup>23</sup> Distances for  $(Cr_{0.038}V_{0.962})_2O_3$  in the PI phase were measured by Dernier<sup>26</sup> using XRD and those for the AFI phase of pure  $V_2O_3$  are calculated from the monoclinic lattice vectors and atomic positions published by Dernier and Marezio.<sup>23</sup> It is evident that the interatomic distances measured by EXAFS for the PI and AFI phases  $(Al_{0.06}V_{0.94})_2O_3$  are essentially the same. In addition, these distances are in correspondence with, though consistently slightly larger than, those obtained for the AFI phase of pure  $V_2O_3$ , confirming that all insulating phases have essentially the same local structure.

NEXAFS spectra of the O 1s edge in the same Al-doped  $Al_2O_3$  crystal are presented in Fig. 4 (a) and 4(b). Large changes in the spectra are apparent as the sample is rotated from a geometry with  $\vec{E}$  parallel to  $\vec{c}_{hex}$  ( $\vartheta=0^\circ$ ) to one with

$\vec{E}$  perpendicular to  $\vec{c}_{hex}$  ( $\vartheta=90^\circ$ ). It is evident that cooling from the PI to the AFI phase has no significant effect on the spectra or their dependence on angle. These spectra and their angular dependence are similar to those of pure  $V_2O_3$  in its low-temperature AFI phase,<sup>9</sup> but different from those of pure  $V_2O_3$  in its high-temperature PM phase, which has a much weaker angular dependence [Fig. 4(c)].

## DISCUSSION

The EXAFS and O edge soft x-ray absorption measurements presented here consistently show that the structure, at least on a local scale, and the V-O hybridization in the PI and AFI phases of  $(Al, V)_2O_3$  are similar, but distinctly different from the metallic phase. The most obvious difference between the metallic and insulating phases is the anisotropy of the O 1s x-ray absorption spectra, reflecting the V-3d-O-2p hybridization. These findings suggest that the structural change at the MI transition (long or short-range order) is directly connected with the emergence of the insulating state, e.g., via changes of hybridization.

To estimate the effect of purely structural changes on the hybridization, we show in Fig. 5 partial (projected) O 2p<sub>z</sub> and 2p<sub>x,y</sub> densities of states (DOS) predicted by the electronic structure calculations. The V 3d partial DOS predictions for the spin-degenerate cases (see Ref. 4) are in good agreement with those of Mattheiss<sup>30</sup> and Ezhov *et al.*<sup>11</sup> The V 3d and O 2p partial DOS presented in Fig. 5 are very similar for all phases, except for a slight decrease of the O 2p bandwidth in the PI phase as compared to the PM phase. In particular, the experimentally observed optical band gap is not reproduced by the calculations and all phases are predicted to be metallic. These discrepancies between experi-

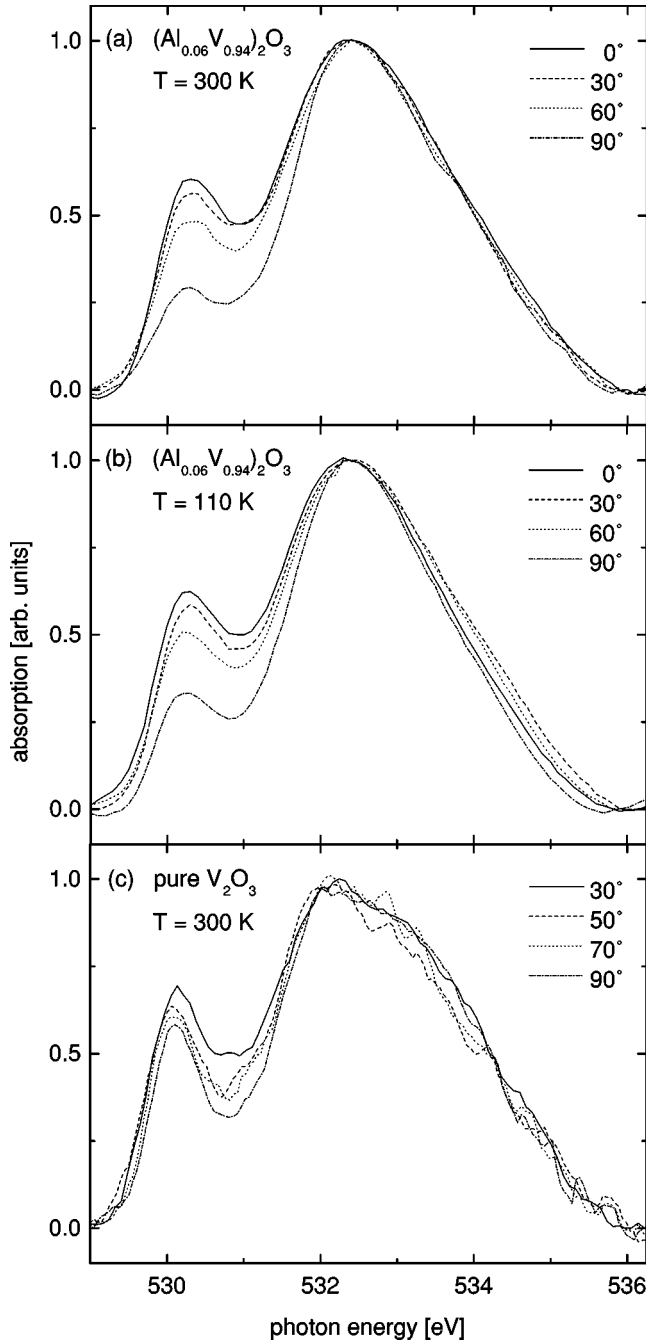


FIG. 4. NEXAFS spectra of the O  $1s$  edge of  $(\text{Al}_{0.06}\text{V}_{0.94})_2\text{O}_3$  as a function of angle between  $\vec{E}$  and the  $c_{hex}$  axis, showing large but identical angular anisotropy for (a) the PI and (b) the AFI phases. For comparison, this angular dependence almost vanishes for pure  $\text{V}_2\text{O}_3$  in its metallic state (c) (from Ref. 9, energy shifted to facilitate comparison). All spectra were normalized to the large maximum at about 532 eV.

ment and calculations are usually attributed to the fact that on-site electron-electron correlations are not fully taken into account by the LDA. The calculations also predict that the O  $2p$  DOS of all phases is isotropic; i.e., the projected  $2p_z$  and  $2p_{x,y}$  DOS are similar, implying that NEXAFS spectra of the O  $1s$  edge with the polarization vector  $\vec{E}$  parallel or perpen-

dicular to  $\vec{c}_{hex}$  should also be alike. Experimentally, this is only observed for the metallic phase of  $\text{V}_2\text{O}_3$ , as shown in Fig. 4(c), but not for the insulating phases. However, the calculations for  $(\text{V}_{0.962}\text{Cr}_{0.038})_2\text{O}_3$  [Fig. 5(b)] described above did not include the local distortions observed by EXAFS in the PI phase and the calculations for monoclinic  $\text{V}_2\text{O}_3$  [Fig. 5(c)] artificially enforced a spin-degenerate state. If the antiferromagnetic ground state of the monoclinic phase is taken into account by using a spin-polarized calculation [Fig. 5(d)], the partial DOS displays various band shifts, although the experimentally observed optical band gap is still not reproduced. In particular, the O  $2p_z$  partial DOS now differs substantially from the  $2p_{x,y}$  near 0.3 eV, 1.7 eV, and 4 eV and is, therefore, more compatible with the observed anisotropy of the O  $1s$  spectra. In this context it should be noted that according to neutron scattering measurements antiferromagnetic short-range order persists in both the PI and PM phases, although the anisotropy of the O  $1s$  spectra is only observed in the PI and AFI phases.

To address the effect of electronic correlations on the electronic structure of  $\text{V}_2\text{O}_3$ , recently the LDA was combined with theory DMFT and calculated and measured photoemission and x-ray absorption spectra were compared on the basis of the calculated V  $3d$  spectral weight.<sup>4</sup> The electron-electron interaction shifts the  $a_{1g}$  and  $e_g^\pi$  states with respect to each other. This would cause an anisotropy in the oxygen  $1s$  spectra, since the  $a_{1g}$  and  $e_g^\pi$  states hybridize differently with the O  $2p_z$  and  $2p_{x,y}$  states. According to the LDA the V  $a_{1g}$  hybridize primarily with the O  $2p_z$  orbital along the  $c_{hex}$  axis, while the  $e_g^\pi$  hybridize primarily with the O  $2p_{x,y}$  inplane orbitals. Therefore polarization-dependent excitations of O  $1s$  core electrons into unoccupied O  $2p_z$  and O  $2p_{x,y}$  states, provide information on their hybridization with V  $a_{1g}$  and  $e_g^\pi$  states, respectively. Based on this we concluded earlier<sup>9</sup> that the observed anisotropy in the AFI phase of pure  $\text{V}_2\text{O}_3$  results from an increase in  $a_{1g}$  character in the unoccupied DOS, causing a corresponding increase of weight of O  $p_z$  hybridized states above  $\epsilon_F$ . This interpretation is consistent with the conclusion of Park *et al.*,<sup>10</sup> based on measurements of the V  $L_{2,3}$  edges, that there is an increase in  $e_g^\pi$  occupancy during the transition from the metallic to the insulating state in  $\text{V}_2\text{O}_3$ . On the other hand, the relative shifts of the  $a_{1g}$  and  $e_g^\pi$  states predicted from LDA + DMFT calculations are not sufficient to account for the observed anisotropy of the O  $1s$  spectra in the insulating state.

Recently Shiina *et al.*<sup>12</sup> attributed the monoclinic lattice distortion in the AFI phase to orbital ordering which would make the three originally equivalent magnetic bonds in the  $ab$  plane inequivalent and cause a monoclinic lattice distortion. Evidence for orbital fluctuations in the PI phase was provided by neutron scattering measurements,<sup>7</sup> which showed that magnetic short-range order was limited to nearest-neighbor distances, resulting in a first-order transition from the PI to the AFI phase. Given the results of Ref. 12, orbital fluctuations in the PI phase could cause a dynamic monoclinic distortion. Assuming that the time scale for such fluctuations is long compared to the time scale of the x-ray-absorption process, EXAFS and soft x-ray absorption would

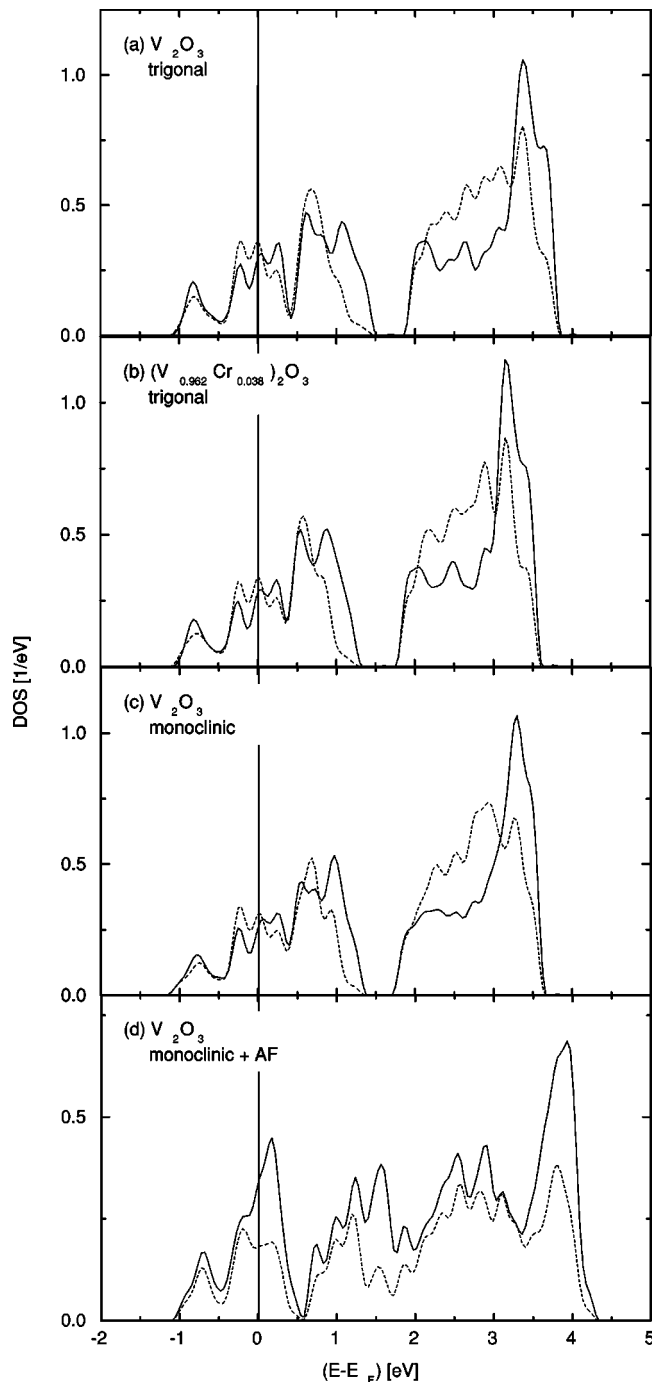


FIG. 5. Partial oxygen  $2p$  densities of states predicted by the density functional calculations described in the text for different crystal structures of  $(V_{1-x}Cr_x)_2O_3$  with various  $c/a$  ratios and symmetries: (a) the trigonal paramagnetic phase ( $x=0$ ), (b) paramagnetic insulating phase with a larger trigonal distortion corresponding to  $x=0.038$ , (c) the monoclinic paramagnetic phase of  $V_2O_3$ , and (d) the monoclinic antiferromagnetic phase. Solid (dashed) lines indicate O  $2p_z$  ( $2p_x$  or  $2p_y$ ) states. For the magnetically ordered phase (d) spin-up and spin-down states have been added to facilitate comparison and the vertical scale has been expanded.

measure an instantaneous structure and the PI phase would appear monoclinic, while XRD, which measures on a much longer time scale, would see a trigonal lattice. In the AFI phase the monoclinic distortion might become static al-

though, on a local scale, still the same as in the PI phase. This model would account for the fact that neither EXAFS nor soft x-ray absorption observe differences between the PI and AFI phases, in contrast to XRD. The spectroscopic results are, however, also consistent with static short-range orbital order in the PI phase, which would, accordingly, be an orbital glass, with an disorder-order transition to the ordered AFI phase.

The local monoclinic distortion we have found in  $(V_{0.94}Al_{0.06})_2O_3$  is reminiscent of the much smaller, but significant monoclinic distortion found in the metallic phase of pure  $V_2O_3$ .<sup>19</sup> From the fact that this monoclinic distortion is not detected in XRD measurements, Frenkel *et al.*<sup>19</sup> set an upper limit of 40 Å on the size of possible monoclinic domains and concluded that the MIT contains both an order-disorder and a displacive component. The monoclinic distortion in the metallic phase was determined to be about 30% of that in the antiferromagnetically ordered insulating phase. From the above discussion it can be concluded that their data suggest that orbital fluctuations are also present in the metallic phase of  $V_2O_3$ , although local distortions are less prominent than in the PI phase, possibly due to better screening in the metallic phase.

## CONCLUSION

The x-ray-absorption measurements presented here show that both the PI and AFI insulating phases of  $V_2O_3$  are distinguished from the PM phase by (i) the presence of local or long-range distortion of the lattice (probably connected to short- or long-range orbital order, respectively) and (ii) differences in the  $V-3d-O-2p$  hybridization, accompanied by corresponding band shifts. Both the distortion and the hybridization appear to be independent of the presence of antiferromagnetic correlations, which are present in all phases.<sup>7</sup> The similarity of the PI and AFI phases, at least on a local scale, suggests a common route from their insulating behavior to the metallic behavior of the PM phase. Interactions between orbital degrees of freedom, which lead to an orbitally ordered state in the AFI phase and orbital short-range order in the PI phase, appear to be an important fingerprint of the MIT. The characteristic differences between  $V-3d-O-2p$  hybridization in the metallic and insulating phases suggest that those changes in hybridization play a role in the MIT. Such changes might be due to strong anharmonic contributions to the temperature-dependent phonon spectrum.

## ACKNOWLEDGMENTS

We appreciate valuable assistance in the measurements and analysis from J. Kirkland at NSLS and Ch. Jung and M. Mast at BESSY and enlightening discussions with P. Riseborough and K. -H. Höck. This work was supported in part by the BMBF under Contract No. 0560GWAA, the DFG under Contract Nos. HO-955/2 and SFB484, by U.S. DOE Contract No. DEFG02-91-ER45439. The NSLS is supported by the DOE.

- <sup>1</sup>D.B. McWhan, A. Menth, J.P. Rameika, W.F. Brinkmann, and T. Rice, *Phys. Rev. B* **7**, 1920 (1973).
- <sup>2</sup>D.B. McWhan, J.P. Rameika, and T.M. Rice, *Phys. Rev. Lett.* **23**, 1384 (1969).
- <sup>3</sup>J. Spalek, *J. Solid State Chem.* **88**, 70 (1990).
- <sup>4</sup>K. Held, G. Keller, V. Eyert, D. Vollhardt, and V.I. Anisimov, *Phys. Rev. Lett.* **86**, 5345 (2001).
- <sup>5</sup>M.J. Rozenberg, G. Kotliar, H. Kajueter, G.A. Thomas, D.H. Rapkine, J.M. Honig, and P. Metcalf, *Phys. Rev. Lett.* **75**, 105 (1995).
- <sup>6</sup>C. Castellani, C.R. Natoli, and J. Ranninger, *Phys. Rev. B* **18**, 4945 (1978); **18**, 4967 (1978); **18**, 5001 (1978).
- <sup>7</sup>W. Bao, C. Broholm, G. Aeppli, S.A. Carter, P. Dai, T.F. Rosenbaum, J.M. Honig, P. Metcalf, and S.F. Trevino, *Phys. Rev. B* **58**, 12 727 (1998).
- <sup>8</sup>W. Bao, C. Broholm, G. Aeppli, P. Dai, J.M. Honig, and P. Metcalf, *Phys. Rev. Lett.* **78**, 507 (1997).
- <sup>9</sup>O. Müller, J.P. Urbach, E. Goering, T. Weber, R. Barth, H. Schuler, M. Klemm, S. Horn, and M.L. denBoer, *Phys. Rev. B* **56**, 15 056 (1997).
- <sup>10</sup>J.-H. Park, L.H. Tjeng, A. Tanaka, C.T. Chen, P. Metcalf, J.M. Honig, F.M.F. de Groot, and G.A. Sawatzky, *Phys. Rev. B* **61**, 11 506 (2000).
- <sup>11</sup>S.Y. Ezhov, V.I. Anisimov, D.I. Khomskii, and G.A. Sawatzky, *Phys. Rev. Lett.* **83**, 4136 (1999).
- <sup>12</sup>R. Shiina, F. Mila, F.-C. Zhang, and T.M. Rice, *Phys. Rev. B* **63**, 144422 (2001).
- <sup>13</sup>F. Mila, R. Shiina, F.-C. Zhang, A. Joshi, M. Ma, V.I. Anisimov, and T.M. Rice, *Phys. Rev. Lett.* **85**, 1714 (2000).
- <sup>14</sup>G.M. Joshi, H.V. Keer, H. Kuwamoto, and J.M. Honig, *Indian J. Pure Appl. Phys.* **15**, 471 (1977).
- <sup>15</sup>F.W. Lytle, R.B. Greeger, D.R. Sandstrom, E.C. Marques, J. Wong, C.L. Spiro, G.P. Huffman, and F.E. Huggins, *Nucl. Instrum. Methods Phys. Res. A* **226**, 542 (1984).
- <sup>16</sup>L. Tröger, D. Arvanatis, K. Baberschke, H. Michaelis, U. Grimm, and E. Zschech, *Phys. Rev. B* **46**, 3283 (1992).
- <sup>17</sup>P. Pfalzer, J.-P. Urbach, M. Klemm, S. Horn, M.L. denBoer, A.I. Frenkel, and J.P. Kirkland, *Phys. Rev. B* **60**, 9335 (1999).
- <sup>18</sup>J. Goulon, C. Goulon-Ginet, R. Cortes, and J.M. Dubois, *J. Phys. (Paris)* **43**, 539 (1982).
- <sup>19</sup>A.I. Frenkel, E.A. Stern, and F.A. Chudnovsky, *Solid State Commun.* **102**, 637 (1997).
- <sup>20</sup>A.L. Ankudinov, B. Ravel, J.J. Rehr, and S.D. Conradson, *Phys. Rev. B* **58**, 7565 (1998).
- <sup>21</sup>R. W. G. Wyckoff, *Crystal Structure* (Interscience, New York, 1963).
- <sup>22</sup>J. -P. Urbach, diploma thesis, Universität Augsburg, 1995.
- <sup>23</sup>P.D. Dernier and M. Marezio, *Phys. Rev. B* **2**, 3771 (1970).
- <sup>24</sup>A.R. Williams, J. Kübler, and C.D. Gelatt, Jr., *Phys. Rev. B* **19**, 6094 (1979).
- <sup>25</sup>V. Eyert, *Int. J. Quant. Chem.* **77**, 1007 (2000).
- <sup>26</sup>P.D. Dernier, *J. Phys. Chem. Solids* **31**, 2569 (1970).
- <sup>27</sup>Use of the crystal structure of Cr-doped V<sub>2</sub>O<sub>3</sub> for the paramagnetic insulating phase is justified by the observation that Cr doping has very similar effects as Al doping and is equivalent to the application of (negative) pressure.
- <sup>28</sup>V. Eyert and K.-H. Höck, *Phys. Rev. B* **57**, 12 727 (1998).
- <sup>29</sup>V. Eyert, *J. Comput. Phys.* **124**, 271 (1996).
- <sup>30</sup>L.F. Mattheiss, *J. Phys.: Condens. Matter* **6**, 6477 (1994).